Lithuanian Journal of Physics
Vol. **65**, No. 4, pp. 248–257 (2025)
ISSN 1648-8504 eISSN 2424-3647
DOI: https://doi.org/10.3952/physics.2025.65.4.7

HOT CARRIER TRANSPORT IN SOLAR CELLS

S. Ašmontas, J. Gradauskas, A. Čerškus, A. Sužiedėlis, E. Širmulis, and O. Žalys

State Research Institute Center for Physical Sciences and Technology, Saulėtekio 3, 10257 Vilnius, Lithuania
Email: steponas.asmontas@ftmc.lt

Received 20 November 2025; accepted 20 November 2025

The study presents the findings on photovoltage formation in solar cells subjected to pulsed laser excitation. Transient photovoltage measurements reveal that the photoresponse comprises two components with opposite polarities, expressed as $U = U_f + U_{ph}$. The fast component, which mirrors the laser pulse profile, arises from the heating of charge carriers by the incident light. In contrast, the slow component corresponds to the conventional photovoltage generated through electron–hole pair creation. The detrimental effect of hot carriers on the power conversion efficiency of perovskite solar cells can be alleviated by reducing band bending near the charge transport layers or by adopting a multijunction cell architecture. This approach enhances spectral utilization and minimizes thermalization losses.

Keywords: hot carriers, solar cell, photovoltage, p-n junction

1. Introduction

Global electricity demands are fuelling the fast growth of the renewable energy industry, and along with it, the technological advances that make these sustainable alternatives more dependable, efficient and cost-effective. One of the most promising and environmentally friendly energy sources is electricity generated by solar cells (SCs). Currently, nearly 90% of solar cells worldwide are produced from silicon [1]. Therefore, it is very important to further improve the performance of silicon solar cells and reduce their cost. The power conversion efficiency (PCE) of a single-junction silicon SC reaches 27.6% [2]. However, it is significantly lower than the theoretical Shockley–Queisser (S–Q) limit of 33.3% [3, 4]. In recent years, various technologies and methods have been developed to improve the power conversion efficiency of the silicon SCs, including pyramid structures and anti-reflecting coatings. To diminish bulk recombination, high quality silicon wafers are used for SCs fabrication. To reduce surface recombination, surface passivation is employed [1, 5]. The PCE of a single-junction solar cell is limited by the fact that only photons with energy close to the forbidden energy gap are effectively used [6]. Higher-energy photons create electron and hole pairs, and the excess energy is transferred to carriers, which become hot carriers. As a result, the hot-carrier thermoelectromotive force U_f is induced across a solar cell. The polarity of U_f is opposite to the polarity of the classical photovoltage resulting from the generation of electron–hole pairs [7]. Therefore, light-induced carrier heating reduces the power conversion efficiency of a SC [6]. For the first time, the thermoelectromotive force of hot carriers was observed across a germanium p-n junction during illumination with CO_2 laser radiation [8]. Later, the thermoelectromotive force of the hot carriers has been investigated in silicon [9], InSb [10] and GaAs p-n junctions [11].

In 1982, Ross and Nozik suggested the idea of a hot-carrier solar energy converter in which the photogenerated hot carriers are extracted over a narrow range of energies at a rate faster than they dissipate energy to the lattice [12]. Theoretically, the power conversion efficiency of such a converter can reach 66%. Later, numerous theoretical and experimental studies have been conducted on the development of hot-carrier solar cells [13–29].

Despite the efforts of many scientists, hot-carrier solar cells suitable for practical use have not been developed to date.

A detrimental process in the utilization of hot carriers is the repeated scattering of hot electrons and holes with phonons, ultimately leading to their relaxation back to the conduction and valence bands, with their excess energy being dissipated as heat. Therefore, the extremely short cooling time of hot carriers in inorganic semiconductors is the main obstacle to the development of hot-carrier solar cells. At room temperature, the cooling time of hot carriers is on the order of 10^{-12} s [30]. The cooling time of hot carriers in organic inorganic metal halide perovskite films is longer, on the order of 10^{-11} s [23, 31]. Therefore, it was thought that lead halide perovskites are promising candidates for the development of hot-carrier solar cells. Kahman and Loi noted that the power conversion efficiency of approximately 50% appears achievable if the hot carrier cooling time of 1 ns can be attained [26]. Monte Carlo simulations show that the hot phonon bottleneck effect may be the primary mechanism responsible for the slow cooling in metal halide perovskites [32]. The hot phonon bottleneck effect arises from the non-equilibrium population of longitudinal optical phonons under intense electron–hole pair generation by light. A recent study of carrier dynamics in lead-free caesium tin halide perovskites revealed a significantly prolonged hot carrier cooling process, lasting approximately 50 ps, due to the hot phonon bottleneck effect and the formation of large polarons [33].

The second challenge in the development of hot-carrier solar cells is to produce a contact material with a narrow density of states at an appropriate energy level – energy selective contacts. To avoid energy loss of the hot carrier, its extraction time must be significantly less than the cooling time [26]. Quantum mechanical resonant tunnelling structures are most likely to satisfy the requirements of selective energy transmission over a small energy range [22]. The hot-carrier photovoltaic cell comprises an absorber region where photons are absorbed, a resonant tunnelling quantum well acting as a selective energy electron filter, and a collector region with a bandgap wider than the absorber region. Measurements of current–voltage characteristics showed that the observed photocurrent during the illumination of the photovoltaic cell with pulsed laser radiation indicates the presence of hot carrier tunnelling current, which may influence the photovoltaic effect. The slow cooling and highly efficient extraction of hot carriers were noted in colloidal perovskite nanocrystals [23]. It has been reported that the hot electron extraction (up to ~ 83%) from $MAPbBr_3$ nanocrystalline thin films at room temperature was reached using a molecular semiconductor as an energy-selective contact. However, an extremely thin absorber is not suitable for the production of solar cells because they absorb only a small portion of the light. Although many researchers believe that creating a highly efficient hot-carrier solar cell is feasible and a worthy goal to pursue [34], implementing this in practice is very difficult and requires fundamentally new ideas.

In this paper, we present the results of investigations into carrier heating in Si and GaAs p-n junctions induced by laser radiation, as well as the impact of hot carriers on photovoltage formation in perovskite solar cells.

2. Hot carriers in Si and GaAs p-n junctions

The investigated gallium arsenide p-n junction was formed of a 6 μm-thick p-type layer with the hole density 6×10^{17} cm^{-3}, liquid-phase epitaxy-grown on an n-type substrate with the electron density 4×10^{17} cm^{-3}. To create the ohmic contact, a 2 μm-thick p^+-layer with the hole density 2.5×10^{18} cm^{-3} was grown upon a p-type layer. The AuGeNi alloy was deposited on the top and back surfaces of the structure by thermal evaporation, and metallic contacts were fabricated by the lift-off technique followed by rapid thermal annealing. The p-n junction was illuminated from the epitaxial layer side through the window etched in the p^+-layer (Fig. 1). Transient photovoltage measurements were used to study carrier heating by infrared laser radiation. To observe the hot carrier effect in the p-n junction, it is necessary to distinguish the thermoelectromotive force of hot carriers from the classical photovoltage arising from electron–hole pair generation. To this end, a short laser pulse with a duration significantly shorter than the carrier recombination time must be used. In the experiments, the Nd:YAG laser with a wavelength of 1.06 μm and a pulse duration of 15 ns, a repetition rate of 50 Hz and a maximum pulse intensity of 1.1 MW/cm^2 was used. The temporal behaviour of the photovoltage and laser pulse in the nanosecond time scale was recorded by

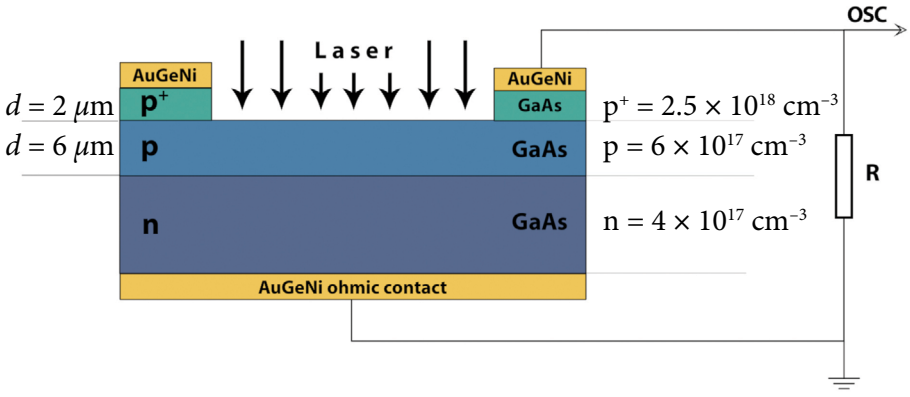

Fig. 1. The structure of the GaAs p-n junction solar cell.

an *Agilent Technologies* digital storage oscilloscope DSO6102A. All measurements were carried out at room temperature.

The temporal shapes of the laser pulse and photovoltage across the GaAs p-n junction under high 1.1 MW/cm^2 intensities of the laser radiation are depicted in Fig. 2. The observed photovoltage U consists of two components having opposite polarities:

$$U = U_f + U_{ph}. \quad (1)$$

Here U_f is a fast component that follows the shape of the laser pulse and is caused by the heating of the charge carriers by light. The polarity of U_f corresponds to the polarity of the thermoelectromotive force of hot carriers [11]. The slow component U_{ph} is the typical photovoltage resulting from electron–hole pair generation during illumination. The dependence of the slow component on laser intensity shows that the magnitude of U_{ph} increases according to the square law (see Fig. 3). This fact indicates that the electron–hole pair generation is determined by the two-photon absorption because the single-photon energy of the Nd:YAG laser is lower than the forbidden energy gap of GaAs. Measurements of the fast component show that U_f linearly depends on the laser intensity at low excitation levels (see Fig. 3). At higher intensities, the dependence of U_f on the laser intensity starts to be sublinear. The deviation of U_f from the linear law is an inherent feature of the thermoelectromotive force of the hot carriers in GaAs [35]. This can be explained by the fact that carrier

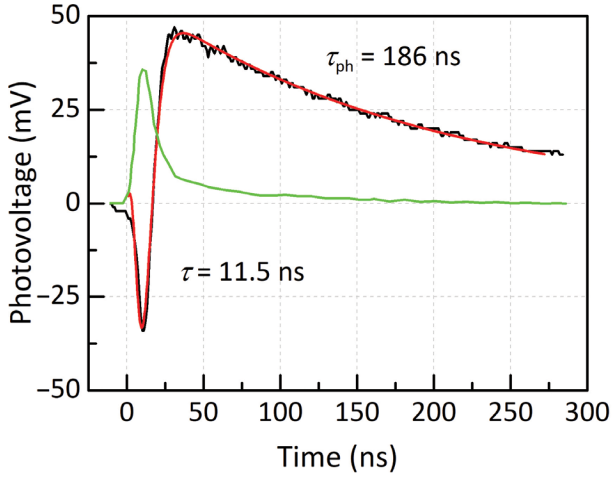

Fig. 2. The oscilloscope traces of the laser pulse (green) and photovoltage (black) of the GaAs p-n junction solar cell. The excitation laser power density I_m = 1.1 MW/cm^2. The red curve represents a fit based on Eqs. (1, 2, 5).

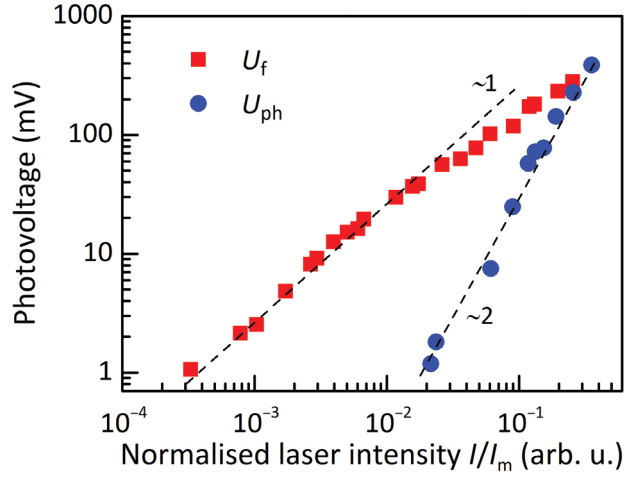

Fig. 3. Variation of the hot-carrier thermoelectromotive force U_f and the classical photovoltage U_{ph} with the normalized laser radiation intensity. The dashed lines serve as visual guides for linear (~1) and quadratic (~2) dependences.

mobility and the diffusion coefficient decrease as carrier energy increases.

At low laser radiation intensities, when the generation of charge carriers is negligible, the photovoltage exhibits only negative polarity, and it consists of two components, the thermoelectromotive force of the hot carriers and the electromotive force due to lattice heating (see Fig. 4). The hot carrier thermoelectromotive force follows the laser pulse and terminates with it. The following slow decrease in photovoltage is due to the cooling of the lattice. The lattice heating-induced electromotive force can be reduced by shortening the laser pulse.

Temporal analysis of the photovoltage can be performed to independently estimate the magnitudes of U_f and U_{ph}. Since the laser pulse duration is much longer than the hot carrier cooling time, the fast component of the photovoltage can be expressed as follows:

$$U_f(t) = K_f \times I(t). \tag{2}$$

Here $I(t)$ is the time-dependent laser pulse intensity, which can be approximated as

$$I(t) = I_m \left(\frac{t}{\tau}\right)^4 \exp\left[4\left(1-\frac{t}{\tau}\right)\right], \tag{3}$$

where I_m is the peak intensity at $t = \tau$, $I_m = I(\tau)$, and τ is the laser rise time. The slow component of the photovoltage $U_{ph}(t)$ can be obtained from

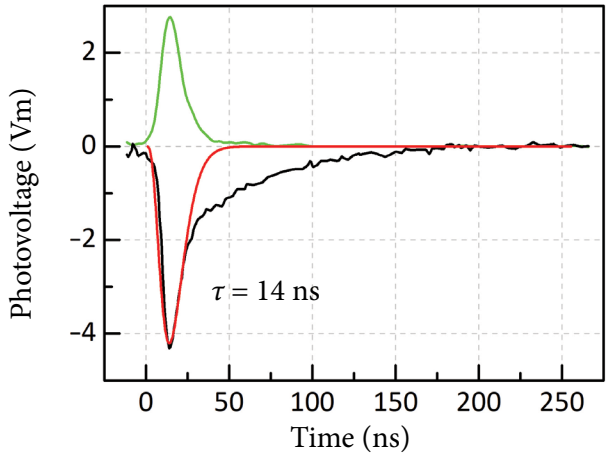

Fig. 4. Experimental trace of the photovoltage (black) and the calculated fast component U_f (red) using Eq. (2) at a low laser excitation level. The green curve represents the laser pulse.

$$\frac{dU_{ph}(t)}{dt} = \frac{\bar{U}_{ph} - U_{ph}(t)}{\tau_{ph}}, \tag{4}$$

where $\bar{U}_{ph} = K_{ph} \times I^2(t)$, and τ_{ph} is the characteristic decay time of $U_{ph}(t)$. The solution of Eq. (4) gives

$$U_{ph}(t) = \frac{8! e^8 K_{ph} I_m^2 \tau}{a^9 \tau_{ph}} \left\{ \exp\left(-\frac{t}{\tau_{ph}}\right) - \left[1 + \sum_{n=1}^{8} \frac{(bt)^n}{n!}\right] \exp\left(-\frac{8t}{\tau}\right) \right\}. \tag{5}$$

Here $a = (8\tau_{ph} - \tau)/\tau_{ph}$ and $b = a/\tau$. The values of the coefficients K_f and K_{ph} can be obtained from the experimental magnitude of the photovoltage at $t = \tau$ and $t = t_m$, respectively. The t_m is defined by $dU_{ph}(t)/dt = 0$ at the moment when $t = t_m$.

The calculated curve using Eqs. (1–5) is shown in Fig. 2. It is seen that the calculated curve coincides with the experimental photovoltage temporal trace. In this way, transient photovoltage measurements, along with the approximations presented above, allow us to separate and quantify both the hot-carrier effect and the electron–hole pair generation-based components of the photovoltage induced across the p-n junction by short-pulse laser radiation.

Experimental study of carrier heating in the silicon p-n junction was carried out using an optical parametric oscillator generating wavelengths from 1.43 to 4.8 μm and is described in detail in Ref. [6]. The investigated p-n junction was produced by chemical vapour deposition of epitaxial p-type silicon on an n-type substrate. The hole density was 6×10^{16} cm^{-3}, and the electron density was 2×10^{16} cm^{-3}, respectively. Ohmic contact to p-Si was formed by boron diffusion into a thin p$^+$-layer at 960°C temperature giving the hole density 8.5×10^{19} cm^{-3}, and subsequent thermal deposition of Al at temperature 320°C and annealing at 560°C in argon atmosphere for 1 min. The Si p-n junction was illuminated from the epitaxial layer side through the window etched in the p$^+$-layer just like in the case of the GaAs p-n junction (see Fig. 1).

Oscilloscope traces of the laser pulse of 1.49 μm wavelength and 25 ns duration and the photovoltage across the Si p-n junction are depicted in Fig. 5. As in the case of GaAs p-n junctions, the photovoltage consists of two components – fast and slow – with

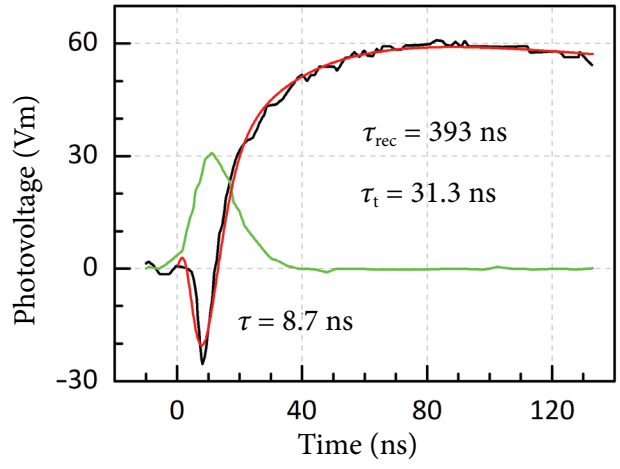

Fig. 5. Oscilloscope traces of the laser pulse (green) and photovoltage (black) across the Si p-n junction. The red curve represents a fit based on Eqs. (1, 2, 7).

opposite polarities. The shape of the fast component follows that of the laser pulse and shares the polarity of the hot-carrier thermoelectromotive force. The slow component is the classical photovoltage due to the generation of electron–hole pairs. Thus, the optical heating of charge carriers leads to a reduction in a single junction solar cell efficiency.

Spectral measurements of the photovoltage show that both U_{ph} and U_f decrease with increasing the wavelength of laser radiation (see Fig. 6). The behaviour of U_{ph} is associated with the decrease of the two-photon absorption coefficient with the wavelength [36]. The slow component of the photovoltage disappears if the wavelength becomes longer than 2.5 μm, i.e. the energy of two photons becomes lower than the forbidden energy gap of Si. In contrast to U_{ph}, the thermoelectromotive force of the hot carriers does not disappear at a longer wavelength because its magnitude is determined by the absorption coefficients of free electrons and free holes [37].

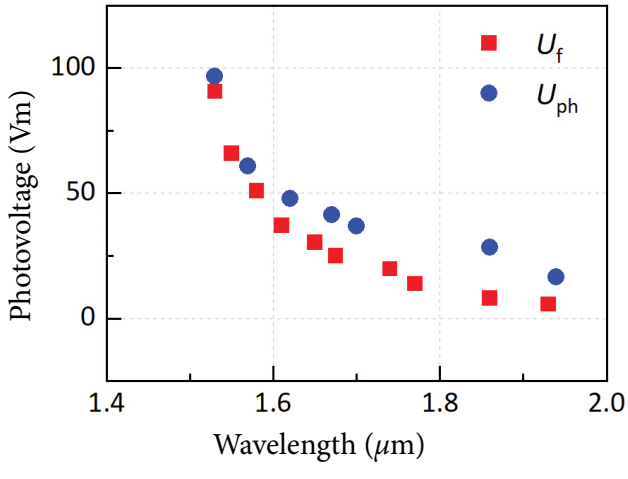

Fig. 6. Variation of the hot-carrier thermoelectromotive force U_f and the classical photovoltage U_{ph} with wavelength at laser power density I_m = 0.25 MW/cm².

3. Hot carriers in perovskite solar cells

The investigated solar cells were fabricated on the basis of caesium-containing triple-cation perovskite layers prepared by the spin-coating method widely described in Refs. [38–40]. Glass substrates of 25 × 25 mm² size coated with a fluorine doped tin oxide layer (FTO) were used for the synthesis of perovskite films. About a 30 nm-thick layer of a compact TiO_2 was formed on the substrates by spraying a solution composed of titanium diisopropoxide (bis) acetylacetonate ($Ti(acac)_2OiPr_2$) and isopropanol (1:9 vol. ratio) and sintering it for 15 min at 450°C on a hotplate. After natural cooling for 6 h, the spin-coating method was used to deposit a 150÷220 nm-thick layer of a mesoporous TiO_2 on the compact TiO_2 layer. The mesoporous TiO_2 was formed by sintering the layer in dry air for 30 min at 450°C. The sample was then cooled down to 150°C and immediately placed in a controlled atmosphere glove box. The perovskite structures were grown on mesoporous TiO_2 using the one-step precipitation method from the prepared precursor's solution. To deposit the perovskite layer on the formed mesoporous TiO_2, the sample was placed on a centrifuge table, and 150 μl of the prepared precursor's solution was dropped with an Eppendorf pipette. Then, the spin program – consisting of two steps – was initiated immediately. Before the end of the spin-coating programme, 150 μl of chlorbenzene was dropped on the surface of the sample to remove the residual solution. Subsequently, the samples were transferred from the centrifuge table to a hot plate and annealed in an inert atmosphere for 60 min at 100°C. After annealing and natural cooling, a hole transport layer – Spiro-OMeTAD – covering the perovskite layer was formed. To measure the current–voltage characteristics of the formed perovskite cells, Au contacts were applied by means of thermal evaporation in the vacuum chamber of *VAKSIS* PVD Vapor-5S Th. A schematic cross-section of

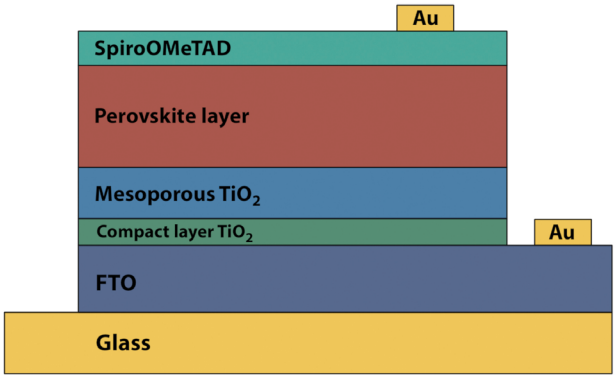

Fig. 7. Schematic structure of the perovskite solar cell.

the perovskite solar cell and the contacts on the top of Spiro-OMeTAD and FTO are presented in Fig. 7.

The morphology and thickness of the formed solar cell were examined using scanning electron microscopy (SEM). Top-view and cross-sectional SEM images of the perovskite layer are shown in Fig. 8. The surface is seen to be flat, pinhole-free and smooth, which is consistent with other reports elsewhere [41, 42]. The composition of the investigated triple-cation perovskite layer containing caesium was $Cs_{0.1}(FA_{0.83}MA_{0.17})_{0.9}Pb(I_{0.83}Br_{0.17})_3$.

A laser pulse of 7 ns duration and 532 nm wavelength was used for illumination. Typical temporal profiles of laser pulse and transient photovoltage induced across a perovskite solar cell are depicted in Fig. 9. It is seen that photovoltage consists of two components, as previously observed in the case of Si and GaAs p-n junctions. The duration of the fast component aligns well with that of the laser pulse. Its polarity coincides with that of the thermoelectromotive force of hot carriers. Thus, it can be assumed that the fast component of the photovoltage arises as a result of free carrier heating by laser radiation, and can be described by Eq. (2).

The thermoelectromotive force of hot carriers arises in perovskite solar cells due to the existence of energy band bending and the corresponding potential barriers near the charge-transport layers. The thermoelectromotive force of the hot carriers, as in the case of Schottky junction, is directly proportional to the potential barrier height of the band bending close to the charge transport layers and to the heating of the carriers [43, 44]

$$eU_f = \varphi_b \times \left(\frac{T_h}{T_0} - 1 \right), \tag{6}$$

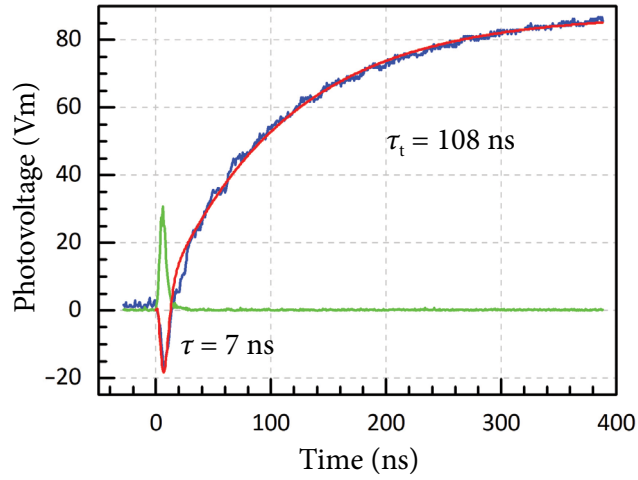

Fig. 9. Temporal shapes of the laser pulse (green) and photovoltage (blue) of the perovskite solar cell. The excitation laser power density I_m = 0.8 MW/cm². The red curve represents a fit based on Eqs. (1, 2, 7).

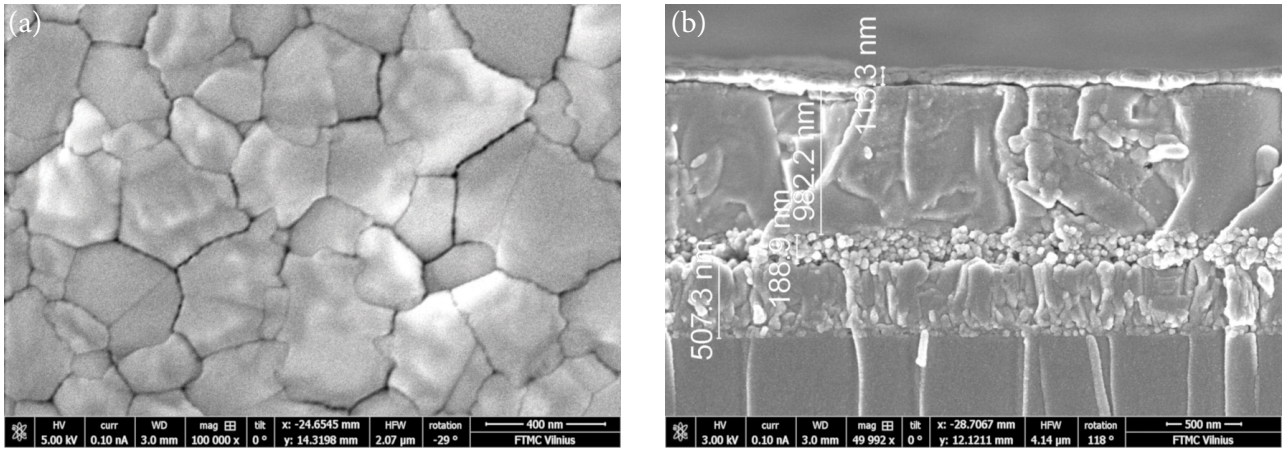

Fig. 8. (a) Top-view and (b) cross-sectional SEM images of the perovskite layer.

where φ_b is the potential barrier height of the band bending, and T_h and T_0 are the temperatures of the hot carriers and the lattice, respectively.

The slow component is the usual photovoltage arising due to electron–hole pair generation, and its form can be expressed as [45]

$$U_{ph}(t) = U_0 \left(\frac{\exp\left(-\frac{t}{\tau_t}\right) - \exp\left(-\frac{t}{\tau_{rec}}\right)}{\frac{1}{\tau_{rec}} - \frac{1}{\tau_t}} \right). \quad (7)$$

Here U_0 represents the initial voltage, τ_t denotes the time constant associated with carrier transport within the perovskite layer, and τ_{rec} refers to the time required for carrier recombination. The calculated dependence of U_{ph} on time is depicted in Fig. 10. The same figure shows the measured photovoltage. It is seen that the measured photovoltage dependence on time can be well described by Eq. (7). This allows us to determine the transit time of the charge carriers across the perovskite layer. The transit time of charge carriers inside the perovskite layer is mainly determined by the diffusion current with the characteristic time constant $\tau_t = d^2/D$, where D is the bipolar diffusion coefficient and d is the film thickness [44, 45]. Knowing the transit time and the thickness of the perovskite layer, the bipolar diffusion coefficient of charge carriers can be determined. For the perovskite layer with d = 982 nm and transit time τ_t = 108 ns, the bipolar diffusion coefficient is 0.089 cm/s.

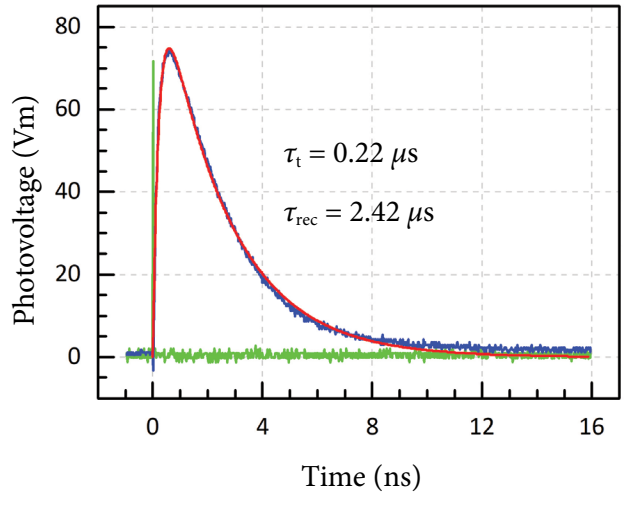

Fig. 10. Oscilloscope traces of the laser pulse (green) and photovoltage across the perovskite solar cell (blue). The red curve is the fit of U_{ph} calculated using Eq. (7). Excitation laser power density I_m = 0.7 MW/cm^2.

This value of D is typical for the spin-coated perovskite layers [39, 44, 46].

4. Conclusions

The experimental investigation of photovoltage formation in solar cells under pulsed laser excitation was conducted. The transient photovoltage measurements reveal that the photoresponse comprises two distinct components: the thermoelectromotive force generated by hot carriers and the classical photovoltage resulting from light-induced electron–hole pair generation. In perovskite solar cells, the magnitude of the hot-carrier thermoelectromotive force is directly proportional to the potential barrier height caused by band bending near the charge transport layers. Carrier heating by light reduces the conversion efficiency of solar cells since the polarity of the hot-carrier thermoelectromotive force opposes that of the classical photovoltage. This detrimental effect can be mitigated by employing multi-junction solar cell architectures [47].

References

[1] C. Yu, S. Xu, J. Yao, and S. Han, Recent advances in and new perspectives on crystalline silicon solar cells with carrier-selective passivation contacts, Crystals **8**(11), 430 (2018), https://doi.org/10.3390/cryst8110430

[2] P. Węgierek, J. Pastuszak, K. Dziadosz, and M. Turek, Influence of substrate type and dose of implanted ions on the electrical parameters of silicon in terms of improving the efficiency of photovoltaic cells, Energies **13**(24), 6708 (2020), https://doi.org/10.3390/en13246708

[3] W. Shockley and H.J. Queisser, Detailed balance limit of efficiency of p-n junction solar cells, J. Appl. Phys. **32**(3), 510–519 (1961), https://doi.org/10.1063/1.1736034

[4] A. Polman, M. Knight, E.C. Garnett, B. Ehrler, and W.C. Sinke, Photovoltaic materials: Present efficiencies and future challenges, Science **352**(6283), aad4424 (2016), https://doi.org/10.1126/science.aad4424

[5] A. Sachenko, V. Kostylyov, I. Sokolovskyi, and M. Evstigneev, Effect of temperature on limit

photoconversion efficiency in silicon solar cells, IEEE J. Photovolt. **10**(1), 63–69 (2020), https://doi.org/10.1109/jphotov.2019.2949418

[6] S. Ašmontas, J. Gradauskas, A. Sužiedėlis, A. Šilėnas, E. Širmulis, V. Švedas, V. Vaičikauskas, and O. Žalys, Hot carrier impact on photovoltage formation in solar cells, Appl. Phys. Lett. **113**(7), 071103 (2018), https://doi.org/10.1063/1.5043155

[7] S. Ašmontas, J. Gradauskas, A. Sužiedėlis, A. Šilėnas, E. Širmulis, V. Vaičikauskas, V. Vaičiūnas, O. Žalys, L. Fedorenko, and L. Bulat, Photovoltage formation across GaAs p–n junction under illumination of intense laser radiation, Opt. Quant. Electron. **48**(9), 448 (2016), https://doi.org/10.1007/s11082-016-0702-z

[8] I. Marmur, Y. Oksman, and A.A. Semenov, Hot carrier current through p-n junction, Phys. Techn. Poluprovodn. **8**, 2216–2217 (1974) [in Russian].

[9] A.V. Andrianov, P.M. Valov, V.L. Sikhanov, V.V. Tuchkevich, and N.M. Shmidt, Hot carrier current through p-n junction, Phys. Techn. Poluprovodn. **14**, 859–864 (1980) [in Russian].

[10] S. Ašmontas, J. Gradauskas, K. Naudžius and E. Širmulis, Photoresponse of InSb-based p-n structures during illumination by CO_2 laser radiation, Phys. Techn. Poluprovodn. **28**, 1089–1091 (1994) [in Russian].

[11] S. Asmontas, J. Gradauskas, D. Seliuta, and E. Sirmulis, Photoelectrical properties of nonuniform semiconductor under infrared laser radiation, in: *Nonresonant Laser-Matter Interaction (NLMI-10)*, Vol. 4423, ed. M. N. Libenson (SPIE 2001) pp. 18–27, https://doi.org/10.1117/12.431223

[12] R.T. Ross and A.J. Nozik, Efficiency of hot-carrier solar energy converters, J. Appl. Phys. **53**(5), 3813–3818 (1982), https://doi.org/10.1063/1.331124

[13] G.J. Conibeer, D. König, M.A. Green, and J.F. Guillemoles, Slowing of carrier cooling in hot carrier solar cells, Thin Solid Films **516**(20), 6948–6953 (2008), https://doi.org/10.1016/j.tsf.2007.12.102

[14] G. Conibeer, N. Ekins-Daukes, J.-F. Guillemoles, D. König, E.-C. Cho, C.-W. Jiang, S. Shrestha, and M. Green, Progress on hot carrier cells, Sol. Energy Mater. Sol. Cells **93**(6–7), 713–719 (2009), https://doi.org/10.1016/j.solmat.2008.09.034

[15] A. Luque and A. Martí, Electron–phonon energy transfer in hot-carrier solar cells, Sol. Energy Mater. Sol. Cells **94**(2), 287–296 (2010), https://doi.org/10.1016/j.solmat.2009.10.001

[16] G. Conibeer, R. Patterson, L. Huang, J.-F. Guillemoles, D. König, S. Shrestha, and M.A. Green, Modelling of hot carrier solar cell absorbers, Sol. Energy Mater. Sol. Cells **94**(9), 1516–1521 (2010), https://doi.org/10.1016/j.solmat.2010.01.018

[17] A. Le Bris and J.-F. Guillemoles, Hot carrier solar cells: Achievable efficiency accounting for heat losses in the absorber and through contacts, Appl. Phys. Lett. **97**(11), 113506 (2010), https://doi.org/10.1063/1.3489405

[18] D. König, K. Casalenuovo, Y. Takeda, G. Conibeer, J. Guillemoles, R. Patterson, L. Huang, and M. Green, Hot carrier solar cells: Principles, materials and design, Physica E **42**(10), 2862–2866 (2010), https://doi.org/10.1016/j.physe.2009.12.032

[19] D.J. Farrell, Y. Takeda, K. Nishikawa, T. Nagashima, T. Motohiro, and N.J. Ekins-Daukes, A hot-carrier solar cell with optical energy selective contacts, Appl. Phys. Lett. **99**(11), 111102 (2011), https://doi.org/10.1063/1.3636401

[20] Y. Takeda and T. Motohiro, Highly efficient solar cells using hot carriers generated by two-step excitation, Sol. Energy Mater. Sol. Cells **95**(9), 2638–2644 (2011), https://doi.org/10.1016/j.solmat.2011.05.023

[21] A.P. Kirk and M.V. Fischetti, Fundamental limitations of hot-carrier solar cells, Phys. Rev. B **86**(16), 165206 (2012), https://doi.org/10.1103/physrevb.86.165206

[22] J.A.R. Dimmock, S. Day, M. Kauer, K. Smith, and J. Heffernan, Demonstration of a hot-carrier photovoltaic cell, Prog. Photovoltaics Res. Appl. **22**(2), 151–160 (2013), https://doi.org/10.1002/pip.2444

[23] M. Li, S. Bhaumik, T.W. Goh, M.S. Kumar, N. Yantara, M. Grätzel, S. Mhaisalkar, N. Mathews, and T.C. Sum, Slow cooling and highly efficient extraction of hot carriers in colloidal perovskite

nanocrystals, Nat. Commun. **8**(1), 14350 (2017), https://doi.org/10.1038/ncomms14350

[24] D.-T. Nguyen, L. Lombez, F. Gibelli, S. Boyer-Richard, A. Le Corre, O. Durand, and J.-F. Guillemoles, Quantitative experimental assessment of hot carrier-enhanced solar cells at room temperature, Nat. Energy **3**(3), 236–242 (2018), https://doi.org/10.1038/s41560-018-0106-3

[25] C.-Y. Tsai, Carrier heating and its effects on the current-voltage relations of conventional and hot-carrier solar cells: A physical model incorporating energy transfer between carriers, photons, and phonons, Sol. Energy **188**, 450–463 (2019), https://doi.org/10.1016/j.solener.2019.06.024

[26] S. Kahmann and M.A. Loi, Hot carrier solar cells and the potential of perovskites for breaking the Shockley–Queisser limit, J. Mater. Chem. C **7**(9), 2471–2486 (2019), https://doi.org/10.1039/c8tc04641g

[27] M. Li, J. Fu, Q. Xu, and T.C. Sum, Slow hot-carrier cooling in halide perovskites: Prospects for hot-carrier solar cells, Adv. Mater. **31**(47), 1802486 (2019), https://doi.org/10.1002/adma.201802486

[28] A.S. Sharma, M. Hanif, S.P. Bremner, M.P. Nielsen, M.J.Y. Tayebjee, F.E. Rougieux, N.J. Ekins-Daukes, and A. Pusch, Heat flow through nonideal contacts in hot-carrier solar cells, Phys. Rev. Appl. **20**(3), 0340001 (2023), https://doi.org/10.1103/PhysRevApplied.20.034001

[29] S. Gogoi, S. Das, R. Gupta, and S.D. Verma, Tuning hot-carrier temperature in $CsPbBr_3$ perovskite nanoplatelets through metal halide passivation, J. Phys. Chem. Lett. **16**(15), 3832–3839 (2025), https://doi.org/10.1021/acs.jpclett.5c00273

[30] S. Ašmontas, Electrogradient phenomena in semiconductors, in: *Electrogradient Phenomena in Semiconductors*, Vol. 5, Electrons in Semiconductors, ed. prof. J. Požela (Mokslas, Vilnius, 1984) [in Russian].

[31] Y. Yang, D.P. Ostrowski, R.M. France, K. Zhu, J. van de Lagemaat, J.M. Luther, and M.C. Beard, Observation of a hot-phonon bottleneck in lead-iodide perovskites, Nature Photon. **10**(1), 53–59 (2015), https://doi.org/10.1038/nphoton.2015.213

[32] T. Faber, L. Filipovic, and L. Koster, The hot phonon bottleneck effect in metal halide perovskites, J. Phys. Chem. Lett. **15**(51), 12601–12607 (2024), https://doi.org/10.1021/acs.jpclett.4c03133

[33] J. Tan, Y. Zhou, X. Feng, X. Cao, Y. Xi, Y. Wu, D. Lu, T. Han, Y. Huang, and X. Xu, Long-range hot carrier transport in lead-free cesium tin halide perovskite microplates, Appl. Phys. Lett. **125**(25), 251102 (2024), https://doi.org/10.1063/5.0243080

[34] A.J. Nozik, Utilizing hot electrons, Nat. Energy **3**(3), 170–171 (2018), https://doi.org/10.1038/s41560-018-0112-5

[35] S. Ašmontas and A. Sužiedėlis, Electrical properties of small area n-n^+ junction, Lith. J. Phys. **33**, 45–51 (1993).

[36] A.D. Bristow, N. Rotenberg, and H.M. van Driel, Two-photon absorption and Kerr coefficients of silicon for 850–2200 nm, Appl. Phys. Lett. **90**(19), 191104 (2007), https://doi.org/10.1063/1.2737359

[37] A. Dargys and J. Kundrotas, *Handbook on Physical Properties of Ge, Si, GaAs, and InP* (Science and Encyclopedia Publishers, Vilnius, 1994).

[38] M. Saliba, T. Matsui, J.-Y. Seo, K. Domanski, J.-P. Correa-Baena, M.K. Nazeeruddin, S.M. Zakeeruddin, W. Tress, A. Abate, A. Hagfeldt, and M. Grätzel, Cesium-containing triple cation perovskite solar cells: improved stability, reproducibility and high efficiency, Energy Environ. Sci. **9**(6), 1989–1997 (2016).

[39] T. Singh and T. Miyasaka, Stabilizing the efficiency beyond 20% with a mixed cation perovskite solar cell fabricated in ambient air under controlled humidity, Adv. Energy Mater. **8**(3), 1700677 (2018), https://doi.org/10.1002/aenm.201700677

[40] S. Ašmontas, A. Čerškus, J. Gradauskas, A. Grigucevičienė, K. Leinartas, A. Lučun, K. Petrauskas, A. Selskis, A. Sužiedėlis, E. Širmulis, and R. Juškėnas, Cesium-containing triple cation perovskite solar cells, Coatings **11**(3), 279 (2021), https://doi.org/10.3390/coatings11030279

[41] X. Sun, J. Xu, L. Xiao, J. Chen, B. Zhang, J. Yao, and S. Dai, Influence of the porosity of the TiO_2 film on the performance of the perovskite solar cell, Int. J. Photoenergy **2017**(1), 4935265 (2017), https://doi.org/10.1155/2017/4935265

[42] J. Wang, X. Zou, J. Zhu, J. Cheng, D. Chen, X. Bai, Y. Yao, C. Chang, X. Yu, B. Liu, Z. Zhou, and G. Li, Effect of optimization of TiO_2 electron transport layer on performance of perovskite solar cells with rough FTO substrates, Materials **13**(10), 2272 (2020), https://doi.org/10.3390/ma13102272

[43] S. Ašmontas and A. Olekas, Thermoelectromotive force and diffusion of hot electrons in metal semiconductor Schottky barrier, Phys. Tech. Semicond. **14**, 2196 (1980).

[44] M. Mujahid, A. Čerškus, J. Gradauskas, A. Grigucevičienė, R. Giraitis, K. Leinartas, A. Lučun, K. Petrauskas, A. Selskis, A. Sužiedėlis, A. Šilėnas, E. Širmulis, and S. Ašmontas, Unveiling the influence of hot carriers on photovoltage formation in perovskite solar cells, Materials (Basel) **18**(1), 85 (2025), https://doi.org/10.3390/ma18010085

[45] R. Hidayat, A.A. Nurunnizar, A. Fariz, Herman, E.S. Rosa, Shobih, T. Oizumi, A. Fujii, and M. Ozaki, Revealing the charge carrier kinetics in perovskite solar cells affected by mesoscopic structures and defect states from simple transient photovoltage measurements, Sci. Rep. **10**(1), 19197 (2020), https://doi.org/10.1038/s41598-020-74603-x

[46] P. Ščajev, C. Qin, R. Aleksiejūnas, P. Baronas, S. Miasojedovas, T. Fujihara, T. Matsushima, C. Adachi, and S. Juršėnas, Diffusion enhancement in highly excited $MAPbI_3$ perovskite layers with additives, J. Phys. Chem. Lett. **9**(12), 3167–3172 (2018), https://doi.org/10.1021/acs.jpclett.8b01155

[47] M. Mujahid, J. Gradauskas, A. Sužiedėlis, E. Širmulis, and S. Ašmontas, Recent advancements in understanding hot carrier dynamics in perovskite solar cells, Energies **18**(13), 3543 (2025), https://doi.org/10.3390/en18133543

KARŠTŲJŲ KRŪVININKŲ PERNAŠA SAULĖS ELEMENTUOSE

S. Ašmontas, J. Gradauskas, A. Čerškus, A. Sužiedėlis, E. Širmulis, O. Žalys

Fizinių ir technologijos mokslų centras, Vilnius, Lietuva

Santrauka

Straipsnyje pateikiami fotoįtampos susidarymo saulės elementuose tyrimų rezultatai, esant impulsiniam lazeriniam sužadinimui. Pereinamosios fotoįtampos matavimai rodo, kad fotoatsakas *U* saulės elementuose susideda iš dviejų priešingo poliškumo dedamųjų: U_f ir U_{ph}. Spartųjį fotoatsako sandą lemia šviesos kaitinami krūvininkai, jis atkartoja lazerio impulso formą, o lėtasis sandas yra tipinė fotoįtampa, atsirandanti dėl elektronų ir skylių porų generacijos. Karštųjų krūvininkų neigiamą poveikį perovskito saulės elementų energijos konversijai galima sušvelninti mažinant energinių juostų užlinkimą šalia krūvio pernašos sluoksnių arba naudojant daugiasandūrinius saulės elementų darinius, kurie efektyviau išnaudoja saulės spektrą ir sumažina šiluminius energijos nuostolius.